

Article

Synthesis, Hydration Processes and Ionic Conductivity of Novel Gadolinium-Doped Ceramic Materials Based on Layered Perovskite BaLa₂In₂O₇ for Electrochemical Purposes

Nataliia Tarasova ^{1,2,*} , Anzhelika Bedarkova ^{1,2}, Irina Animitsa ^{1,2}  and Evgeniya Verinkina ²

¹ The Institute of High Temperature Electrochemistry, Ural Branch of the Russian Academy of Sciences, 620066 Ekaterinburg, Russia

² Institute of Hydrogen Energy, Ural Federal University, Mira St. 19, 620000 Yekaterinburg, Russia

* Correspondence: natalia.tarasova@urfu.ru

Abstract: The search for novel highly effective materials with target properties for different electrochemical purposes is active for now. Ceramic materials with high levels of ionic conductivity can be applied as electrolytic materials in solid oxide fuel cells and in electrolyzers. Layered perovskites are a novel class of ionic conductors demonstrating almost-pure proton transportation at mid-temperatures. Gadolinium-doped ceramic materials based on layered perovskite BaLa₂In₂O₇ were obtained and investigated for the first time in this study. The effect of the dopant concentrations on the hydration processes and on ionic conductivity was revealed. It was shown that compositions $0 \leq x \leq 0.15$ of BaLa_{2-x}Gd_xIn₂O₇ exhibited proton conductivity when under wet air and at mid-temperatures (lower than ~450 °C). Gadolinium doping led to an increase in the conductivity values up to an order of magnitude of ~0.5. The protonic conductivity of the most conductive composition BaLa_{1.85}Gd_{0.15}In₂O₇ was $2.7 \cdot 10^{-6}$ S/cm at 400 °C under wet air. The rare earth doping of layered perovskites is a prospective approach for the design of ceramics for electrochemical devices for energy applications.

Keywords: BaLa₂In₂O₇; layered perovskite; Ruddlesden-Popper structure; proton conductivity



Citation: Tarasova, N.; Bedarkova, A.; Animitsa, I.; Verinkina, E. Synthesis, Hydration Processes and Ionic Conductivity of Novel Gadolinium-Doped Ceramic Materials Based on Layered Perovskite BaLa₂In₂O₇ for Electrochemical Purposes. *Processes* **2022**, *10*, 2536. <https://doi.org/10.3390/pr10122536>

Academic Editor: Yury Zaikov

Received: 14 November 2022

Accepted: 28 November 2022

Published: 29 November 2022

Publisher's Note: MDPI stays neutral with regard to jurisdictional claims in published maps and institutional affiliations.



Copyright: © 2022 by the authors. Licensee MDPI, Basel, Switzerland. This article is an open access article distributed under the terms and conditions of the Creative Commons Attribution (CC BY) license (<https://creativecommons.org/licenses/by/4.0/>).

1. Introduction

The search of novel highly effective materials with target properties for different electrochemical purposes is active for now. One of the main goals of modern humanity is the creation of highly effective, low-cost, eco-friendly and safe energy sources [1–3]. Hydrogen energy perfectly satisfies these characteristics, and its development is now a very high priority [4–7]. For full function in hydrogen energy systems, the creation of devices for the production, storage and transportation of hydrogen is required [8–10]. Devices such as protonic ceramic electrolysis cells and protonic ceramic fuel cells use electrochemical technologies to obtain hydrogen and for clean energy production [11–16]. Ceramic materials with a high level of ionic conductivity can be applied as electrolytic materials in solid oxide fuel cells and in electrolyzers [17–23]. The proton-conducting materials used for these purposes must have a high chemical resistance to carbon dioxide and water vapor and must exhibit high values of proton conductivity at the same time. Achieving a combination of all these characteristics in one material is a difficult task, so the material search continues.

Hexagonal perovskites [24,25] and layered perovskites [26,27] have been studied as proton-conducting materials in recent years. Layered perovskites may be represented by the formula AA'_nB_nO_{3n+1}, where A is a bivalent metal (alkali-earth metal), A' is a trivalent metal (rare-earth metal) and B is a trivalent metal (indium, scandium) with a smaller ionic radius compared with the radius of the A' cation. The protonic conductivities of these materials, such as BaNdInO₄ [28–32], SrLaInO₄ [33–37], BaNdScO₄ [38], BaLaInO₄, is

realized due to the possibility of dissociative water intercalation into the interlayer space of the layered structure. The monolayer barium-lanthanum indate BaLaInO_4 was described as a nearly pure proton conductor below $400\text{ }^\circ\text{C}$, and an increase in the conductivity values up to 1.5 orders of magnitude caused by heterovalent [39–42] and isovalent [43–46] doping was revealed. The two-layer composition $\text{BaLa}_2\text{In}_2\text{O}_7$ of this homologous series $\text{AA}'_n\text{B}_n\text{O}_{3n+1}$ was also described as a protonic conductor [47]. The possibility of water uptake was proved, and the use of the acceptor-doping strategy made it possible to significantly increase the proton conductivity [48–50]. However, the isovalent-doping strategy for the modification of the structure and transportation properties has not been applied to the two-layer perovskite $\text{BaLa}_2\text{In}_2\text{O}_7$ yet. In this work, gadolinium-doped ceramic materials based on the layered perovskite $\text{BaLa}_2\text{In}_2\text{O}_7$ were obtained and investigated for the first time. The effect of the dopant concentrations on the hydration processes and on ionic conductivity was revealed.

2. Materials and Methods

The samples of $\text{BaLa}_{2-x}\text{Gd}_x\text{In}_2\text{O}_7$ were synthesized using solid state method. The starting reagents BaCO_3 , La_2O_3 , In_2O_3 and Gd_2O_3 were used. The final temperature of calcination was $1300\text{ }^\circ\text{C}$.

The XRD investigations were performed using a Bruker D8 Advance $\text{Cu K}\alpha$ diffractometer (step of 0.01° , scanning rate of $0.5^\circ/\text{min}$). The thermogravimetry (TG) was performed using STA 409 PC NETZSCH analyzer. The heating of initially hydrated samples was performed in the temperature range of $40\text{--}1100\text{ }^\circ\text{C}$ at the rate of $10\text{ }^\circ\text{C}/\text{min}$ under a flow of dry Ar. The hydrated samples were obtained during slow cooling ($1\text{ }^\circ\text{C}/\text{min}$) from 1100 to $150\text{ }^\circ\text{C}$ under a flow of wet Ar.

The electrical conductivity was measured using impedance spectrometer Z-1000P, Elinx, RF. The investigations were performed from 1000 to $200\text{ }^\circ\text{C}$ with $1^\circ/\text{min}$ cooling rate under dry air or dry Ar conditions. The dry gas (air or Ar) was produced by circulating the gas through P_2O_5 ($p_{\text{H}_2\text{O}} = 3.5 \cdot 10^{-5}\text{ atm}$). The wet gas (air or Ar) was obtained by bubbling the gas at room temperature first through distilled water and then through saturated solution of KBr ($p_{\text{H}_2\text{O}} = 2 \cdot 10^{-2}\text{ atm}$).

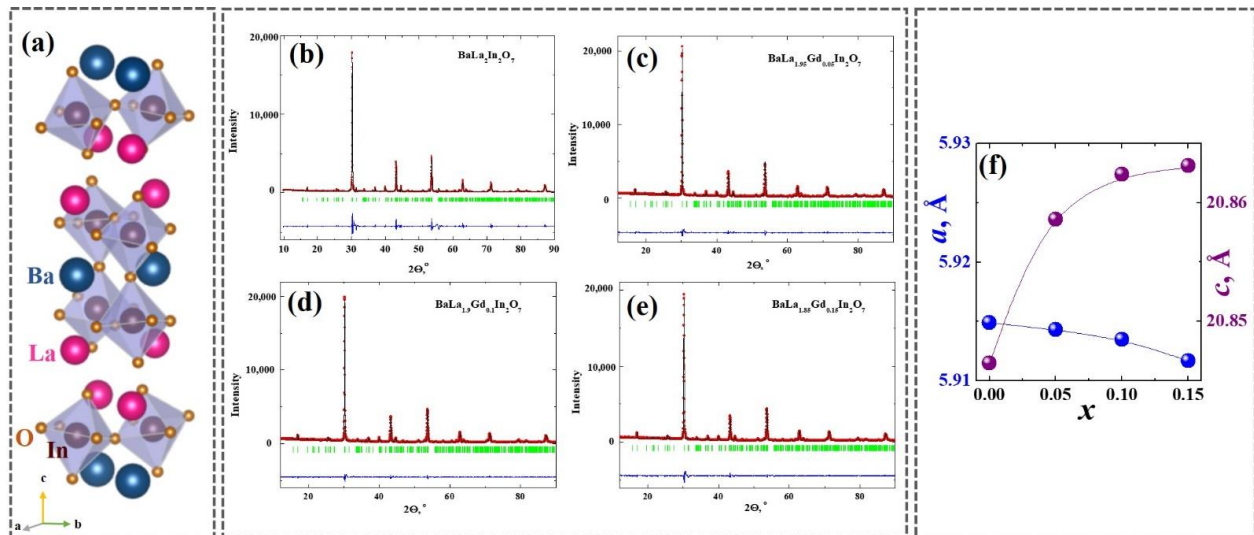
3. Results

The phase attestation of the solid solution of $\text{BaLa}_{2-x}\text{Gd}_x\text{In}_2\text{O}_7$ was performed using the XRD method. It was shown that the compositions at the dopant concentrations $0 \leq x \leq 0.15$ were in a single phase and were isostructural to the matrix composition $\text{BaLa}_2\text{In}_2\text{O}_7$ (Figure 1a). The samples from the solid solution's homogeneity region had a tetragonal symmetry and belonged to the space group $P4_2/mnm$. The XRD-patterns of the obtained compositions are presented in Figure 1b–d. Table 1 contains the lattice parameters and unit cell volumes of the compositions.

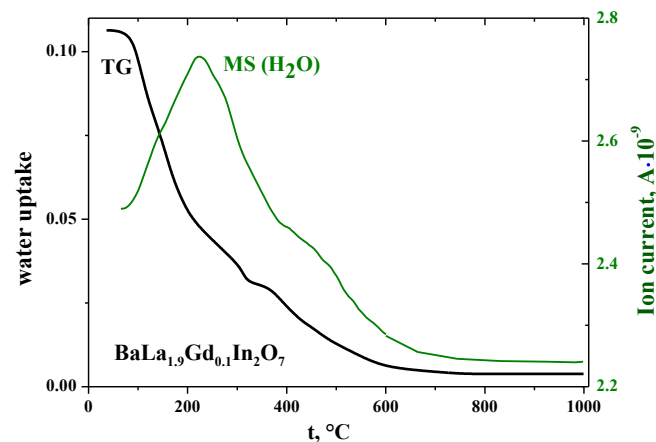
As can be seen, the introduction of an ion with a slightly smaller ionic radius ($r_{\text{La}^{3+}} = 1.216\text{ \AA}$; $r_{\text{Gd}^{3+}} = 1.107\text{ \AA}$ [51]) led to a decrease in lattice parameter a but also to an increase in lattice parameter c (Figure 1e). Therefore, the unit cell volume almost did not change. It was obvious that the reason for these changes was the interatomic distance during doping, which is not only the difference in the ionic radii of the ions but also the difference in their electronegativity. The electronegativities of lanthanum and gadolinium were different ($\chi_{\text{La}} = 1.10$; $\chi_{\text{Gd}} = 1.20$ [52]), which caused the occurrence of additional repulsion effects between these cations when in the same crystallographic positions of the crystal lattice. This could be probable because of the increase in the c lattice parameter during doping. It should be noted that the same increase in the lattice parameters during gadolinium doping occurred for the monolayer composition BaLaInO_4 [45].

Table 1. The lattice parameters and unit cell volumes of investigated compositions of $\text{BaLa}_{2-x}\text{Gd}_x\text{In}_2\text{O}_7$.

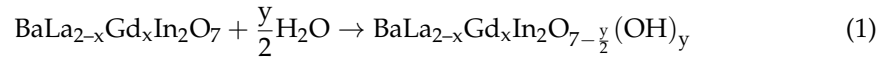
Composition	a , Å	c , Å	V , Å ³
$\text{BaLa}_2\text{In}_2\text{O}_7$	5.914(9)	20.846(5)	729.33(6)
$\text{BaLa}_{1.95}\text{Gd}_{0.05}\text{In}_2\text{O}_7$	5.914(3)	20.858(6)	729.61(1)
$\text{BaLa}_{1.9}\text{Gd}_{0.1}\text{In}_2\text{O}_7$	5.913(5)	20.862(4)	729.54(7)
$\text{BaLa}_{1.85}\text{Gd}_{0.15}\text{In}_2\text{O}_7$	5.911(7)	20.863(1)	729.00(0)

**Figure 1.** (a) Crystal structure of $\text{BaLa}_2\text{In}_2\text{O}_7$ and (f) the concentration dependencies of the lattice parameters. XRD-patterns of (b) $\text{BaLa}_2\text{In}_2\text{O}_7$, (c) $\text{BaLa}_{1.95}\text{Gd}_{0.05}\text{In}_2\text{O}_7$, (d) $\text{BaLa}_{1.9}\text{Gd}_{0.1}\text{In}_2\text{O}_7$ and (e) $\text{BaLa}_{1.85}\text{Gd}_{0.15}\text{In}_2\text{O}_7$ compositions.

The possibility of water uptake from the gas phase was investigated using the thermogravimetry (TG) method. The TG-curves for all of the investigated samples had the same shape, and the results for the composition $\text{BaLa}_{1.9}\text{Gd}_{0.1}\text{In}_2\text{O}_7$ are presented in Figure 2 as an example. Water loss occurred in several steps and ended at 600–700 °C. The mass spectroscopy (MS) results (the green line in Figure 2) confirmed the TG-data. The values of the water uptake of the doped compositions were in the range 0.10–0.13 mol per formula unit, which was comparable to the water uptake of the undoped composition (0.17 mol [47]).

**Figure 2.** Thermogravimetry (TG) and mass spectrometry (MS) results for the composition $\text{BaLa}_{1.9}\text{Gd}_{0.1}\text{In}_2\text{O}_7$.

We could suppose that very small changes in the unit cell volume that occurred during doping caused these small changes in the water uptake. Despite the relatively small water uptake, the possibility for the dissociative incorporation of water into the crystal lattice of the gadolinium-doped compositions indicated the possibility of protonic transport. The interaction of the investigated compositions with water molecules can be described as:



The electrical conductivity values were obtained using the impedance spectroscopy method in the atmospheres with controlled humidity ($p\text{H}_2\text{O}$) and an oxygen partial pressure ($p\text{O}_2$). Figure 3 represents the temperature dependencies of the conductivities obtained under dry air (Figure 3a), dry Ar (Figure 3b), wet air (Figure 3c) and wet Ar (Figure 3d).

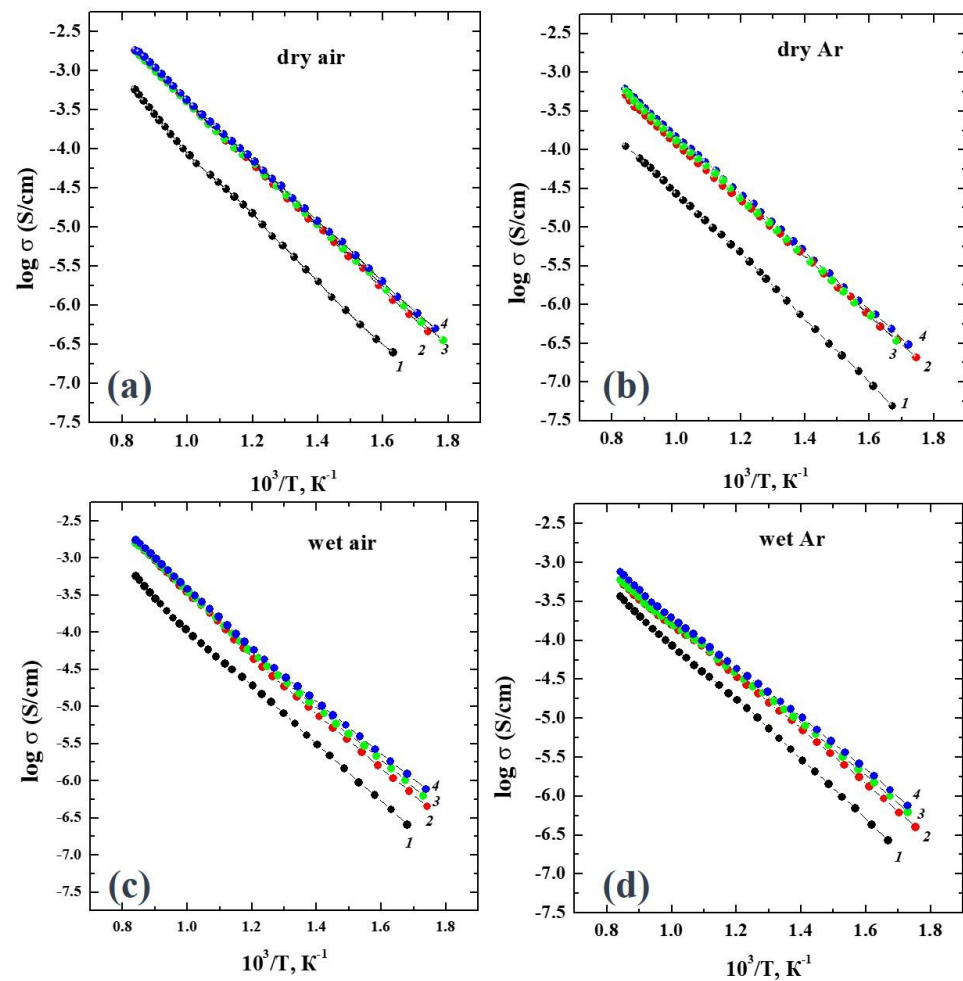


Figure 3. The temperature dependencies of conductivities for the compositions of $\text{BaLa}_{2-x}\text{Gd}_x\text{In}_2\text{O}_7$ at $x = 0$ (1), $x = 0.05$ (2), $x = 0.10$ (3) and $x = 0.15$ (4) obtained under (a) dry air, (b) dry Ar, (c) wet air and (d) wet Ar.

As can be seen, an increase in the gadolinium concentration led to an increase in the electrical conductivity regardless of the values of $p\text{H}_2\text{O}$ and $p\text{O}_2$. The concentration dependencies (Figure 4a) were well illustrated with this regularity. The effect of the changes in the $p\text{H}_2\text{O}$ and $p\text{O}_2$ on the conductivity values at the same dopant concentrations is presented in Figure 4b. The values obtained under dry Ar ($p\text{O}_2 \sim 10^{-5}$ atm) were lower than those obtained under dry air ($p\text{O}_2 = 0.21$ atm), which indicated the mixed oxygen-hole nature of the conductivity. The effect of the humidity changes was more visible in the Ar atmosphere, where the conductivity values under wet conditions ($p\text{H}_2\text{O} = 2 \cdot 10^{-2}$ atm) were

significantly increased compared with those under dry conditions ($p_{\text{H}_2\text{O}} = 3.5 \cdot 10^{-5}$ atm). This indicated the appearance of a proton contribution to the conductivity.

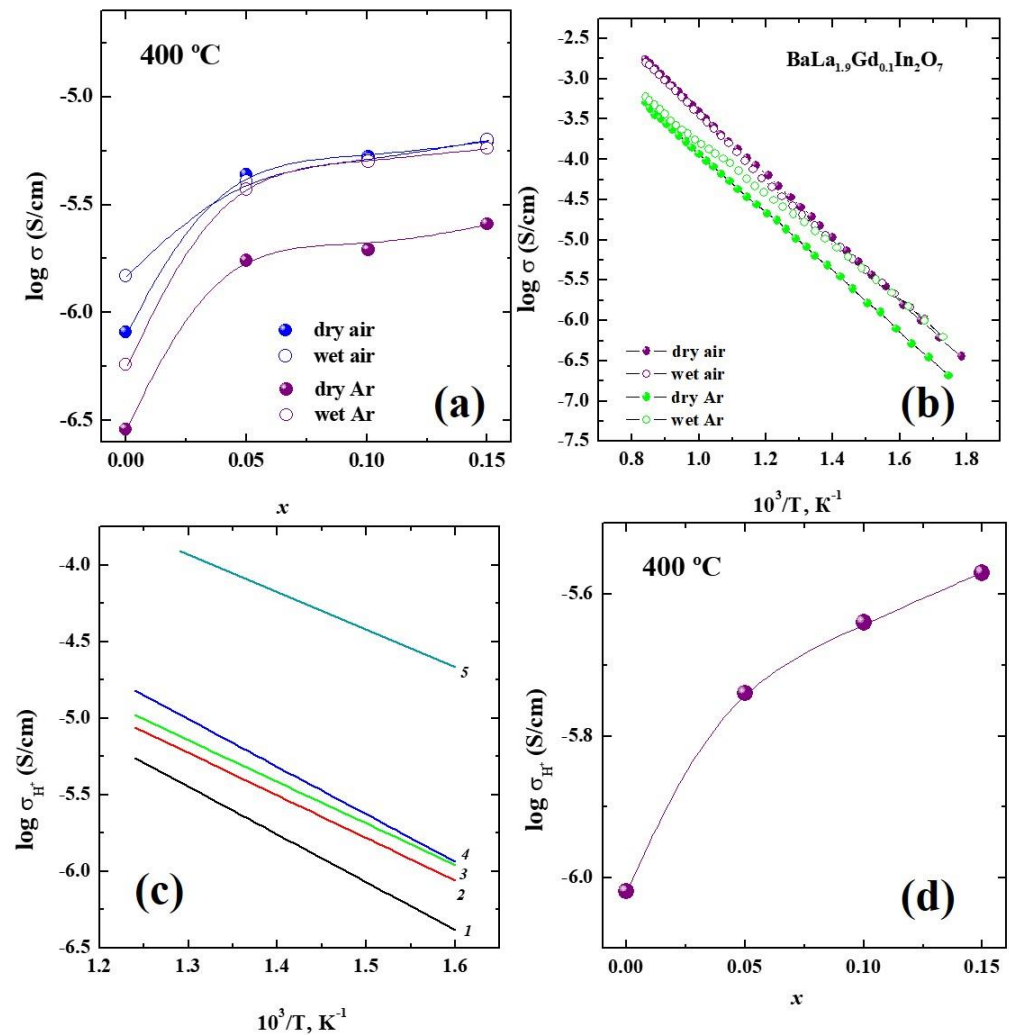


Figure 4. (a) The concentration dependencies and (b) temperature dependencies of conductivities for the compositions of $\text{BaLa}_{2-x}\text{Gd}_x\text{In}_2\text{O}_7$ obtained under different conditions. (c) The temperature dependencies and (d) concentration dependency of protonic conductivities of the compositions of $\text{BaLa}_{2-x}\text{Gd}_x\text{In}_2\text{O}_7$ with $x = 0$ (1), $x = 0.05$ (2), $x = 0.10$ (3) and $x = 0.15$ (4) and for the composition $\text{BaLa}_{1.7}\text{Ba}_{0.3}\text{In}_2\text{O}_{6.85}$ (5).

The protonic conductivity can be calculated as the differences between the ionic conductivities under wet and dry conditions, i.e., between conductivities obtained under wet and dry Ar. The temperature dependencies of the protonic conductivities of the $\text{BaLa}_{2-x}\text{Gd}_x\text{In}_2\text{O}_7$ compositions are presented in Figure 4c. Doping led to an increase in the conductivity values (Figure 4d) up to an order of magnitude of ~ 0.5 for the mostly conductive composition $\text{BaLa}_{1.85}\text{Gd}_{0.15}\text{In}_2\text{O}_7$. In general, this increase in the electrical conductivity values was due to the increase in the concentration of the current carriers and their mobility. In the case of oxygen-ionic conductivity, the concentration of the oxygen point defects did not change during the gadolinium doping of the lanthanum sublattice (isovalent doping). However, the oxygen-ionic conductivity values (the conductivities obtained under dry Ar) increased with the increase of the dopant concentrations. The most reasonable cause was the increase in the oxygen mobility with the increase of the gadolinium content. The lattice parameter c increased, which indicated the increase in the interlayer space in the crystal structure, so the free migration volume increased, which

could facilitate ion transportation, i.e., the increase in the oxygen mobility. In the case of the protonic conductivity, the water uptake (i.e., the proton concentration) was almost the same for all the compositions of $\text{BaLa}_{2-x}\text{Gd}_x\text{In}_2\text{O}_7$; thus, the main reason for the protonic conductivity increase during doping was the increase in the proton mobility. Due to the fact that proton transportation is carried out by the jumping of protons onto oxygen atoms, an increase in the oxygen mobility should have led to the increase in the protonic mobility.

The comparison of the protonic conductivities of the investigated composition obtained by isovalent doping and of the acceptor-doped composition $\text{BaLa}_{1.7}\text{Ba}_{0.3}\text{In}_2\text{O}_{6.85}$ is presented in Figure 4c. The composition $\text{BaLa}_{1.7}\text{Ba}_{0.3}\text{In}_2\text{O}_{6.85}$ was chosen as the most proton-conductive compound obtained by the heterovalent doping of the matrix composition $\text{BaLa}_2\text{In}_2\text{O}_7$ [48]. As can be seen, the protonic conductivity values for the acceptor-doped composition were higher than those for the isovalent-doped compositions by about one order of magnitude. Because the values of the water uptake for the acceptor-doped (~ 0.2 mol) and isovalent-doped (~ 0.13 mol) compositions were comparable to each other, we could suggest that the different proton mobilities were the most reasonable explanation for the significant difference in the protonic conductivity values. The lattice parameter c (20.954(9) Å) and the unit cell volume (743.50(2) Å³) of the acceptor-doped composition $\text{BaLa}_{1.7}\text{Ba}_{0.3}\text{In}_2\text{O}_{6.85}$ were much larger than those of the isovalent-doped composition $\text{BaLa}_{1.85}\text{Gd}_{0.15}\text{In}_2\text{O}_7$ (20.863(1) Å and 729.00(0) Å³). Obviously, this increase provided the facilitation of proton transportation, which led to the increase in the protonic mobility and the conductivity. We suggested that choosing the isovalent dopant with a larger ionic radius than lanthanum would increase the conductivity more significantly.

Summarizing all the obtained results, we could say that the isovalent-doping strategy of the layered perovskite $\text{BaLa}_2\text{In}_2\text{O}_7$ was a successful way to improve the proton conductivity. Gadolinium doping led to an increase in the lattice parameter c , which led to an increase in the ionic transportation in the layered structure. The protonic conductivity increased with the increasing dopant content. The protonic conductivity of the most conductive composition $\text{BaLa}_{1.85}\text{Gd}_{0.15}\text{In}_2\text{O}_7$ was $2.7 \cdot 10^{-6}$ S/cm at 400 °C under wet air.

4. Conclusions

The isovalent-doping strategy for the modification of the structure and transportation properties of the two-layer perovskite $\text{BaLa}_2\text{In}_2\text{O}_7$ was applied for the first time. The gadolinium-doped ceramic materials $\text{BaLa}_{2-x}\text{Gd}_x\text{In}_2\text{O}_7$ were obtained and investigated. The effect of the dopant concentrations on the hydration processes and the ionic conductivity was revealed. It was shown that all of the compositions exhibited proton conductivity under wet air and at mid-temperatures (lower than ~ 450 °C). Gadolinium doping led to an increase in the conductivity values up to an order of magnitude of ~ 0.5 . The protonic conductivity of the most conductive composition $\text{BaLa}_{1.85}\text{Gd}_{0.15}\text{In}_2\text{O}_7$ was $2.7 \cdot 10^{-6}$ S/cm at 400 °C under wet air. The rare earth doping of layered perovskites is a prospective approach for the design of ceramics for electrochemical devices for energy applications.

Author Contributions: Conceptualization, I.A. and N.T.; methodology, I.A. and N.T.; investigation, A.B. and E.V.; data curation, A.B.; writing—original draft preparation, N.T.; writing—review and editing, N.T. and I.A. All authors have read and agreed to the published version of the manuscript.

Funding: This research received no external funding.

Data Availability Statement: Not applicable.

Conflicts of Interest: The authors declare no conflict of interest.

References

1. Malerba, D. Poverty-energy-emissions pathways: Recent trends and future sustainable development goals. *Int. J. Sustain. Energy Dev.* **2019**, *49*, 109–124. [[CrossRef](#)]
2. Buonomano, A.; Barone, G.; Forzano, C. Advanced energy technologies, methods, and policies to support the sustainable development of energy, water and environment systems. *Energy Rep.* **2022**, *8*, 4844–4853. [[CrossRef](#)]
3. Olabi, A.G.; Abdelkareem, M.A. Renewable energy and climate change. *Renew. Sustain. Energy Rev.* **2022**, *158*, 112111. [[CrossRef](#)]

4. Østergaard, P.A.; Duic, N.; Noorollahi, Y.; Mikulcic, H.; Kalogirou, S. Sustainable development using renewable energy technology. *Renew. Energy* **2020**, *146*, 2430–2437. [[CrossRef](#)]
5. International Energy Agency. *The Future of Hydrogen: Seizing Today's Opportunities*; OECD: Paris, French, 2019. [[CrossRef](#)]
6. Abdalla, A.M.; Hossain, S.; Nisfindy, O.B.; Azad, A.T.; Dawood, M.; Azad, A.K. Hydrogen production, storage, transportation and key challenges with applications: A review. *Energy Convers. Manag.* **2018**, *165*, 602–627. [[CrossRef](#)]
7. Dawood, F.; Anda, M.; Shafiullah, G.M. Hydrogen production for energy: An overview. *Int. J. Hydrog. Energy* **2020**, *45*, 3847–3869. [[CrossRef](#)]
8. Scovell, M.D. Explaining hydrogen energy technology acceptance: A critical review. *Int. J. Hydrog. Energy* **2022**, *47*, 10441–104591. [[CrossRef](#)]
9. Lebrouhi, B.E.; Djoupo, J.J.; Lamrani, B.; Benabdelaziz, K.; Kousksou, T. Global hydrogen development—A technological and geopolitical overview. *Int. J. Hydrog. Energy* **2022**, *47*, 7016–7048. [[CrossRef](#)]
10. Arsad, A.Z.; Hannan, M.A.; Al-Shetwi, A.Q.; Mansur, M.; Mittaqui, K.M.; Dong, Z.Y.; Blaabjerg, F. Hydrogen energy storage integrated hybrid renewable energy systems: A review analysis for future research directions. *Int. J. Hydrog. Energy* **2022**, *47*, 17285–17312. [[CrossRef](#)]
11. Meng, Y.; Gao, J.; Zhao, Z.; Amoroso, J.; Tong, J.; Brinkman, K.S. Review: Recent progress in low-temperature proton-conducting ceramics. *J. Mater. Sci.* **2019**, *54*, 9291–9312. [[CrossRef](#)]
12. Medvedev, D. Trends in research and development of protonic ceramic electrolysis cells. *Int. J. Hydrog. Energy* **2019**, *44*, 26711–26740. [[CrossRef](#)]
13. Medvedev, D.A. Current drawbacks of proton-conducting ceramic materials: How to overcome them for real electrochemical purposes. *Curr. Opin. Green Sustain. Chem.* **2021**, *32*, 100549. [[CrossRef](#)]
14. Zvonareva, I.; Fu, X.-Z.; Medvedev, D.; Shao, Z. Electrochemistry and energy conversion features of protonic ceramic cells with mixed ionic-electronic electrolytes. *Energy Environ. Sci.* **2022**, *15*, 439–465. [[CrossRef](#)]
15. Chiara, A.; Giannici, F.; Pipitone, C.; Longo, A.; Aliotta, C.; Gambino, M.; Martorana, A. Solid-Solid Interfaces in Protonic Ceramic Devices: A Critical Review. *ACS Appl. Mater. Interfaces* **2020**, *12*, 55537–55553. [[CrossRef](#)]
16. Cao, J.; Ji, Y.; Shao, Z. New Insights into the Proton-Conducting Solid Oxide Fuel Cells. *J. Chin. Ceram. Soc.* **2021**, *49*, 83–92. [[CrossRef](#)]
17. Shim, J.H. Ceramics breakthrough. *Nat. Energy* **2018**, *3*, 168–169. [[CrossRef](#)]
18. Bello, I.T.; Zhai, S.; He, Q.; Cheng, C.; Dai, Y.; Chen, B.; Zhang, Y.; Ni, M. Materials development and prospective for protonic ceramic fuel cells. *Int. J. Energy Res.* **2021**, *46*, 2212–2240. [[CrossRef](#)]
19. Irvine, J.; Rupp, J.L.M.; Liu, G.; Xu, X.; Haile, S.; Qian, X.; Snyder, A.; Freer, R.; Ekren, D.; Skinner, S.; et al. Roadmap on inorganic perovskites for energy applications. *J. Phys. Energy* **2021**, *3*, 031502. [[CrossRef](#)]
20. Hossain, S.; Abdalla, A.M.; Jamain, S.N.B.; Zaini, J.H.; Azad, A.K. A review on proton conducting electrolytes for clean energy and intermediate temperature-solid oxide fuel cells. *Renew. Sustain. Energy Rev.* **2017**, *79*, 750–764. [[CrossRef](#)]
21. Kim, J.; Sengodan, S.; Kim, S.; Kwon, O.; Bu, Y.; Kim, G. Proton conducting oxides: A review of materials and applications for renewable energy conversion and storage. *Renew. Sustain. Energy Rev.* **2019**, *109*, 606–618. [[CrossRef](#)]
22. Zhang, W.; Hu, Y.H. Progress in proton-conducting oxides as electrolytes for low-temperature solid oxide fuel cells: From materials to devices. *Energy Sci. Eng.* **2021**, *9*, 984–1011. [[CrossRef](#)]
23. Kasyanova, A.V.; Zvonareva, I.A.; Tarasova, N.A.; Bi, L.; Medvedev, D.A.; Shao, Z. Electrolyte materials for protonic ceramic electrochemical cells: Main limitations and potential solutions. *Mater. Rep. Energy*, 2022; 100158, *in press*. [[CrossRef](#)]
24. Fop, S.; McCombie, K.S.; Wildman, E.J.; Skakle, J.M.S.; Irvine, J.T.S.; Connor, P.A.; Savaniu, C.; Ritter, C.; McLaughlin, A.C. High oxide ion and proton conductivity in a disordered hexagonal perovskite. *Nat. Mater.* **2020**, *19*, 752–757. [[CrossRef](#)]
25. Yashima, M.; Tsujiguchi, T.; Sakuda, Y.; Yasui, Y.; Zhou, Y.; Fujii, K.; Torii, S.; Kamiyama, T.; Skinner, S.J. High oxide-ion conductivity through the interstitial oxygen site in Ba₇Nb₄MoO₂₀-based hexagonal perovskite related oxides. *Nat. Comm.* **2021**, *12*, 556. [[CrossRef](#)]
26. Tarasova, N.; Animitsa, I. Materials A^{II}LnInO₄ with Ruddlesden-Popper structure for electrochemical applications: Relationship between ion (oxygen-ion, proton) conductivity, water uptake and structural changes. *Materials* **2022**, *15*, 114. [[CrossRef](#)]
27. Tarasova, N.; Animitsa, I.; Galisheva, A.; Medvedev, D. Layered and hexagonal perovskites as novel classes of proton-conducting solid electrolytes: A focus review. *Electrochem. Mater. Technol.* **2022**, *1*, 20221004. [[CrossRef](#)]
28. Fujii, K.; Shiraiwa, M.; Esaki, Y.; Yashima, M.; Kim, S.J.; Lee, S. Improved oxide-ion conductivity of NdBaInO₄ by Sr doping. *J. Mater. Chem. A* **2015**, *3*, 11985–11990. [[CrossRef](#)]
29. Ishihara, T.; Yan, Y.; Sakai, T.; Ida, S. Oxide ion conductivity in doped NdBaInO₄. *Solid State Ion.* **2016**, *288*, 262–265. [[CrossRef](#)]
30. Yang, X.; Liu, S.; Lu, F.; Xu, J.; Kuang, X. Acceptor doping and oxygen vacancy migration in layered perovskite NdBaInO₄-based mixed conductors. *J. Phys. Chem. C* **2016**, *12*, 6416–6426. [[CrossRef](#)]
31. Fujii, K.; Yashima, M. Discovery and development of BaNdInO₄—A brief review. *J. Ceram. Soc. Jpn.* **2018**, *126*, 852–859. [[CrossRef](#)]
32. Zhou, Y.; Shiraiwa, M.; Nagao, M.; Fujii, K.; Tanaka, I.; Yashima, M.; Bague, L.; Basbus, J.F.; Moggi, L.V.; Skinner, S.J. Protonic conduction in the BaNdInO₄ structure achieved by acceptor doping. *Chem. Mater.* **2021**, *33*, 2139–2146. [[CrossRef](#)] [[PubMed](#)]
33. Kato, S.; Ogasawara, M.; Sugai, M.; Nakata, S. Synthesis and oxide ion conductivity of new layered perovskite La_{1-x}Sr_{1+x}InO_{4-d}. *Solid State Ion.* **2002**, *149*, 53–57. [[CrossRef](#)]

34. Troncoso, L.; Alonso, J.A.; Aguadero, A. Low activation energies for interstitial oxygen conduction in the layered perovskites $\text{La}_{1+x}\text{Sr}_{1-x}\text{InO}_{4+d}$. *J. Mater. Chem. A* **2015**, *3*, 17797–17803. [[CrossRef](#)]
35. Troncoso, L.; Alonso, J.A.; Fernández-Díaz, M.T.; Aguadero, A. Introduction of interstitial oxygen atoms in the layered perovskite $\text{LaSrIn}_{1-x}\text{B}_x\text{O}_{4+\delta}$ system (B = Zr, Ti). *Solid State Ion.* **2015**, *282*, 82–87. [[CrossRef](#)]
36. Troncoso, L.; Mariño, C.; Arce, M.D.; Alonso, J.A. Dual oxygen defects in layered $\text{La}_{1.2}\text{Sr}_{0.8-x}\text{Ba}_x\text{InO}_{4+d}$ ($x = 0.2, 0.3$) oxide-ion conductors: A neutron diffraction study. *Materials* **2019**, *12*, 1624. [[CrossRef](#)]
37. Troncoso, L.; Arce, M.D.; Fernández-Díaz, M.T.; Moggi, L.V.; Alonso, J.A. Water insertion and combined interstitial-vacancy oxygen conduction in the layered perovskites $\text{La}_{1.2}\text{Sr}_{0.8-x}\text{Ba}_x\text{InO}_{4+d}$. *New J. Chem.* **2019**, *43*, 6087–6094. [[CrossRef](#)]
38. Shiraiwa, M.; Kido, T.; Fujii, K.; Yashima, M. High-temperature proton conductors based on the (110) layered perovskite BaNdScO_4 . *J. Mat. Chem. A* **2021**, *9*, 8607–8619. [[CrossRef](#)]
39. Tarasova, N.; Animitsa, I.; Galisheva, A. Effect of acceptor and donor doping on the state of protons in block-layered structures based on BaLaInO_4 . *Solid State Comm.* **2021**, *323*, 114093. [[CrossRef](#)]
40. Tarasova, N.; Galisheva, A.; Animitsa, I. Improvement of oxygen-ionic and protonic conductivity of BaLaInO_4 through Ti doping. *Ionics* **2020**, *26*, 5075–5088. [[CrossRef](#)]
41. Tarasova, N.; Galisheva, A.; Animitsa, I. $\text{Ba}^{2+}/\text{Ti}^{4+}$ —Co-doped layered perovskite BaLaInO_4 : The structure and ionic (O^{2-} , H^+) conductivity. *Int. J. Hydrog. Energy* **2021**, *46*, 16868–16877. [[CrossRef](#)]
42. Tarasova, N.; Galisheva, A.; Animitsa, I.; Belova, K. Simultaneous hetero- and isovalent doping as the strategy for improving transport properties of proton conductors based on BaLaInO_4 . *Materials* **2021**, *14*, 6240. [[CrossRef](#)] [[PubMed](#)]
43. Tarasova, N.; Galisheva, A.; Animitsa, I.; Korona, D.; Davletbaev, K. Novel proton-conducting layered perovskite based on BaLaInO_4 with two different cations in B-sublattice: Synthesis, hydration, ionic (O^{2+} , H^+) conductivity. *Int. J. Hydrog. Energy* **2022**, *47*, 18972–18982. [[CrossRef](#)]
44. Tarasova, N.; Galisheva, A.; Animitsa, I.; Anokhina, I.; Gilev, A.; Cheremisina, P. Novel mid-temperature $\text{Y}^{3+} \rightarrow \text{In}^{3+}$ doped proton conductors based on the layered perovskite BaLaInO_4 . *Ceram. Int.* **2022**, *48*, 15677–15685. [[CrossRef](#)]
45. Tarasova, N.; Bedarkova, A.; Animitsa, I. Proton transport in the gadolinium-doped layered perovskite BaLaInO_4 . *Materials* **2022**, *15*, 7351. [[CrossRef](#)] [[PubMed](#)]
46. Tarasova, N.; Bedarkova, A. Advanced proton-conducting ceramics based on layered perovskite BaLaInO_4 for energy conversion technologies and devices. *Materials* **2022**, *15*, 6841. [[CrossRef](#)] [[PubMed](#)]
47. Tarasova, N.; Galisheva, A.; Animitsa, I.; Korona, D.; Kreimesh, H.; Fedorova, I. Protonic transport in layered perovskites $\text{BaLa}_n\text{In}_n\text{O}_{3n+1}$ ($n = 1, 2$) with Ruddlesden-Popper structure. *Appl. Sci.* **2022**, *12*, 4082. [[CrossRef](#)]
48. Tarasova, N.; Bedarkova, A.; Animitsa, I.; Belova, K.; Abakumova, E.; Cheremisina, P.; Medvedev, D. Oxygen Ion and Proton Transport in Alkali-Earth Doped Layered Perovskites Based on $\text{BaLa}_2\text{In}_2\text{O}_7$. *Inorganics* **2022**, *10*, 161. [[CrossRef](#)]
49. Tarasova, N.A. Local structure and ionic transport in acceptor-doped layered perovskite $\text{BaLa}_2\text{In}_2\text{O}_7$. *Chim. Techno Acta* **2022**, *9*, 20229415. [[CrossRef](#)]
50. Tarasova, N.; Bedarkova, A.; Animitsa, I.; Abakumova, E.; Belova, K.; Kreimesh, H. Novel high conductive ceramic materials based on two-layer perovskite $\text{BaLa}_2\text{In}_2\text{O}_7$. *Int. J. Mol. Sci.* **2022**, *23*, 12813. [[CrossRef](#)]
51. Shannon, R.D. Revised effective ionic radii and systematic studies of interatomic distances in halides and chalcogenides. *Acta Cryst. A* **1976**, *32*, 751–767. [[CrossRef](#)]
52. Allred, A.L. Electronegativity values from thermochemical data. *J. Inorg. Nucl. Chem.* **1961**, *17*, 215–221. [[CrossRef](#)]